Tmprss3, a Transmembrane Serine Protease Deficient in Human DFNB8/10 Deafness, Is Critical for Cochlear Hair Cell Survival at the Onset of Hearing

Lydie Fasquelle, Hamish S Scott, Marc Lenoir, Jing S Wang, Guy Rebillard, Sophie Gaboyard, Stéphanie Venteo, Florence François, Anne-Laure Mausset-Bonnefont, Stylianos E. Antonarakis, et al.

THE JOURNAL OF BIOLOGICAL CHEMISTRY VOL. 286, NO. 19, pp. 17383–17397, May 13, 2011

Tmprss3, a Transmembrane Serine Protease Deficient in Human DFNB8/10 Deafness, Is Critical for Cochlear Hair Cell Survival at the Onset of Hearing*[S]

Received for publication, October 1, 2010, and in revised form, March 14, 2011 Published, JBC Papers in Press, March 21, 2011, DOI 10.1074/jbc.M110.190652

Lydie Fasquelle[‡§¶1], Hamish S. Scott[‖1,2], Marc Lenoir[‡§], Jing Wang[‡§], Guy Rebillard[‡§], Sophie Gaboyard[‡§], Stéphanie Venteo[‡§], Florence François[‡§], Anne-Laure Mausset-Bonnefont[‡§], Stylianos E. Antonarakis[¶], Elizabeth Neidhart[¶], Christian Chabbert[‡§], Jean-Luc Puel[‡§3], Michel Guipponi[¶4], and Benjamin Delprat[‡§4]**

*From [‡]INSERM U 583, Institut des Neurosciences, Hôpital Saint Eloi, 34091 Montpellier, France, the [§]Université de Montpellier, 34091 Montpellier, France, the [¶]Department of Genetic Medicine and Development, University of Geneva Medical School and University Hospitals of Geneva, 1211 Geneva 4, Switzerland, the [‖]Department of Molecular Pathology, the Centre for Cancer Biology, SA Pathology, Box 14 Rundle Mall Post Office, Adelaide, South Australia 5000, Australia, and the **School of Medicine, the School of Molecular and Biomedical Science, University of Adelaide, South Australia 5005, Australia*

Mutations in the type II transmembrane serine protease 3 (*TMPRSS3*) gene cause non-syndromic autosomal recessive deafness (DFNB8/10), characterized by congenital or childhood onset bilateral profound hearing loss. In order to explore the physiopathology of TMPRSS3 related deafness, we have generated an ethyl-nitrosourea-induced mutant mouse carrying a protein-truncating nonsense mutation in *Tmprss3* (Y260X) and characterized the functional and histological consequences of Tmprss3 deficiency. Auditory brainstem response revealed that wild type and heterozygous mice have normal hearing thresholds up to 5 months of age, whereas *Tmprss3*^{Y260X} homozygous mutant mice exhibit severe deafness. Histological examination showed degeneration of the organ of Corti in adult mutant mice. Cochlear hair cell degeneration starts at the onset of hearing, postnatal day 12, in the basal turn and progresses very rapidly toward the apex, reaching completion within 2 days. Given that auditory and vestibular deficits often co-exist, we evaluated the balancing abilities of *Tmprss3*^{Y260X} mice by using rotating rod and vestibular behavioral tests. *Tmprss3*^{Y260X} mice effectively displayed mild vestibular syndrome that correlated histologically with a slow degeneration of saccular hair cells. *In situ* hybridization in the developing inner ear showed that *Tmprss3* mRNA is localized in sensory hair cells in the cochlea and the vestibule. Our results show that Tmprss3 acts as a permissive factor for cochlear hair cells survival and activation at the onset of hearing and is required for saccular hair cell survival. This mouse model will certainly help to decipher the molecular mechanisms underlying DFNB8/10 deafness and cochlear function.

Hearing impairment is the most common sensory defect in humans. Approximately 1 in 1000 newborns is born deaf, and ~50% of these cases of congenital deafness are genetic. Recently, mutations in the *TMPRSS3* gene on chromosome 21q22.3 were shown to cause human autosomal recessive non-syndromic hearing loss (DFNB8/10) (1). *TMPRSS3*-related deafness is characterized by bilateral, severe to profound hearing loss, with no described middle ear or vestibular deficits. Environmental and/or genetic modifiers may influence the expressivity of hearing loss caused by *TMPRSS3* mutations. For instance, missense mutation P404L, altering a highly conserved amino acid of the TMPRSS3 serine protease domain, causes congenital hearing loss in a Tunisian family (2), whereas in a family from Turkey, it leads to childhood onset (6–7 years of age) deafness (2, 3). Clinical presentation of hearing loss resulting from mutations in *TMPRSS3* is indistinguishable from the other forms of non-syndromic recessive non-syndromic hearing loss, and its diagnosis is therefore based on both clinical and molecular evaluation.

TMPRSS3 is a type II transmembrane serine protease, structurally defined by a transmembrane domain located near the N terminus; a low density lipoprotein receptor A domain, which binds calcium (4) and low density lipoprotein (5); a scavenger receptor cysteine-rich domain that is involved in protein-protein interaction (6); and a C-terminal serine protease domain from the S1 family of the SA clan of serine-type peptidases for which the prototype is chymotrypsin (7). Sixteen different TMPRSS3 mutations that lie in all functional domains have been described to date and were found to disrupt the proteolytic activity of TMPRSS3 (8).

RT-PCR and RNA *in situ* hybridization experiments revealed significant *Tmprss3* expression in the thymus, stomach, testis, and embryonic day 19 embryos and in specific cochlear tissues, including the stria vascularis, spiral ganglion neurons, modiolus, organ of Corti, and some cells of the Kölliker's organ (9). It was hypothesized that Tmprss3 may participate in the regulation of sodium homeostasis through its ability to activate the inner ear-expressed sodium channel (ENaC) *in vitro* (9). However, this hypothesis has been challenged by the fact that pseudohypoaldosteronism patients mutated in the *ENaC* gene show

* This work was supported Swiss National Science Foundation Grant 3100A0-114077-1 (to M. G.); National Health and Medical Research Council of Australia Grants 257501, 215305, 71601, and 461204 (to H. S. S.); and a grant from the Région Languedoc-Roussillon (Chercheur d'Avenir) (to B. D.).

[S] The on-line version of this article (available at http://www.jbc.org) contains supplemental Figs. S1–S5.

[1] Both authors contributed equally to this work.
[2] To whom correspondence may be addressed. Tel.: 61-8-8222-3651; Fax: 61-8-8222-3162; E-mail: hamish.scott@health.sa.gov.au.
[3] To whom correspondence may be addressed. Tel.: 33-499636009; Fax: 33-499636020; E-mail: jean-luc.puel@inserm.fr.
[4] Both authors contributed equally to this work.

normal hearing thresholds (10). Therefore, the genuine role of Tmprss3 in the auditory system is currently unknown, and alternative pathways should be explored *in vivo*. Here, we report on the cellular, molecular, and phenotypic characterization of a mouse model for *Tmprss3*-related deafness.

EXPERIMENTAL PROCEDURES

Animal Handling

The care and use of animals followed the animal welfare guidelines of INSERM, under the approval of the French "Ministère de l'Alimentation, de l'Agriculture et de la Pêche". All efforts were made to minimize the number of animals used and their suffering.

Generation of Tmprss3 Mutant Mice; the Tmprss3^{Y260X} Protein-truncating Mutation

Ingenium Pharmaceuticals AG has developed a large library of cryopreserved mutant mouse sperm derived from a chemical mutagenesis program, in which male C3HeB/FeJ mice were mutagenized with ethyl-nitrosourea. The screen for deleterious mutations in the *Tmprss3* gene was performed in G1 animals that were derived from the mating of mutagenenized G0 males with untreated C3HeB/FeJ females. A mutation search was performed using heteroduplex formation analysis by temperature gradient capillary electrophoresis.

Mouse Genotyping

Genomic DNA was prepared from mouse tail tips. PCR amplicons were generated using 10 pmol of each primer (5′-CCCGAGATTTGGCAGTATTG-3′) and 5′-biotin-AGCAGGCCCAGTCACTCAC-3′). The biotinylated PCR product was purified using streptavidin-Sepharose beads (GE Healthcare) and sequenced with primer (5′-CGGCACACTGTGTTTA-3′) using the PSQ 96 SNP reagent kit (Biotage AB, Uppsala, Sweden). Genotype was determined using PyroQ-CpGSoftware (Biotage AB, Uppsala, Sweden).

RT-PCR Analysis of the Tmprss3^{WT} and Tmprss3^{Y260X} Transcript Expression

PCRs and RT-PCRs were performed using primers designed to encompass the Y260X mutation (5′-CCCGAGATTTGGCAGTATTG-3′/5′-AGCAGGCCCAGTCACTCAC-3′ and 5′-CACTCTGTGTACATGAGGGAAGG-3′/5′-TCGGGAAAGTTCTCTTCAGAGTT-3′, respectively). PCR products were sequenced using the ABI Prism Big Dye terminator and run on an ABI 3130XL sequencer.

Preparation of Mouse Inner Ear Extracts

Mouse cochleae were isolated, ground in a mortar, and homogenized manually in a lysis buffer containing antiproteases (Roche Applied Science). The lysis buffer contains 150 mM NaCl, 1% SDS, 1% PMSF, 1 mM EDTA, 10 mM Tris-HCl, pH 7.4. After centrifugation at 10,000 × *g* for 5 min, the supernatants were used for Western blotting.

Western Blot

Polyclonal antibody was raised in rabbit against one peptide, NH_2-CFLDWWIHEQMERDLTK-COOH (amino acids 439–454 of human TMPRSS3; Tmprss3-Cter) (Covalab, Lyon, France). Mouse cochlear extracts were separated on a 8% SDS-PAGE in Tris/glycine. After gel electrophoresis, proteins were transferred electrophoretically onto nitrocellulose membranes (Protan-Whatman, Dassel, Germany). Blots were incubated with Tmprss3-Cter antibody diluted at 1:1000 and revealed by chemiluminescence using a peroxidase-conjugated secondary antibody (ECL, GE Healthcare). A polypeptide range marker was used for calibration (Fermentas GmbH, Mannheim, Germany).

In Situ Hybridization

Total RNA was isolated from the inner ear of wild type mice and reverse transcribed. The fragment was PCR-amplified and subcloned into the pCR4Blunt-TOPO (Invitrogen) with the following primers: Tmprss3his-S2 (5′-GCACAGAAATCATGGGCTCACG-3′) and Tmprss3his-AS (5′- TAGTCATCTCTTACTGTGACTAG-3′). Digoxigenin-labeled probes were synthesized using the Roche Applied Science digoxigenin labeling kit according to the manufacturer's instructions. The probe for peripherin was kindly provided by Dr. M. M. Portier. *In situ* hybridization was carried out as described (11).

Assessment of Hearing Function

Animals were anesthetized by an intraperitoneal injection of a mixture of Rompun 2% (3 mg/kg) and Zoletyl 50 (40 mg/kg). Both pinna were severed to facilitate the insertion and placement of the distortion product otoacoustic emission (DPOAE)[5] probe.

Distortion Product Otoacoustic Emission Recordings—DPOAEs were recorded in the external auditory canal using an ER-10C S/N 2525 probe (Etymotic Research Inc., Elk Grove Village, IL) and consisted of two emitters and one microphone. The two primary tones were generated and the distortion was processed by the Cubdis system HID 40133DP (Mimosa Acoustics Inc., Champaign, IL). The probe was self-calibrated for the two stimulating tones before each recording. The two tones were presented simultaneously, sweeping f2 from 0.5 kHz to 20 kHz by quarter-octave steps and maintaining the f2/f1 ratio constant at 1.2. The primary intensities of f2 and f1 were set at 60 and 55 dB sound pressure level (SPL) (reference 2×10^{-5} pascals), respectively. For each frequency, the cubic distortion product ($2f1 - f2$) and the neighboring noise magnitudes were measured and expressed as a function of f2. Data are expressed as means ± S.E.

Auditory Brainstem Response Recordings—The acoustical stimuli were generated by an arbitrary function generator (type 9100R, LeCroy Corp.), consisting of 9-ms tone bursts with a 1-ms rise and fall time delivered at a rate of 10/s. Tone bursts were passed through a programmable attenuator and delivered to the animal by a JBL 075 loudspeaker (James B. Lansing Sound, Inc., Stamford, CT) in a calibrated free field. The audi-

[5] The abbreviations used are: DPOAE, distortion product otoacoustic emission; SPL, sound pressure level; ABR, auditory brainstem response; SEM, scanning electron microscopy; TEM, transmission electron microscopy; IHC, inner hair cell; OHC, outer hair cell; ER, endoplasmic reticulum; P*n*, postnatal day *n*.

tory brainstem responses (ABRs) were derived from two needle electrodes respectively placed at the vertex and on the mastoid of the stimulated ear. The signal was differentially amplified (×10,000) by a Tektronix (TM 503) differential amplifier and digitized (50 kHz sampling rate, with a 12-bit dynamic range and 1024 samples/burst), averaged 512 times, and stored on a computer (Dell Dimensions, Dell Inc., Round Rock, TX). Intensity-amplitude functions of brainstem responses were obtained at each frequency tested (2, 4, 6, 8, 10, 12, 16, 20, 26, and 32 kHz) by varying the intensities of the tone bursts from 0 to 90 dB SPL, in 5-dB steps. The ABR thresholds were defined as the minimum sound intensity necessary to elicit a clearly distinguishable response.

Endocochlear Potential Measurement—After a ventrolateral approach to the cochlea, the bone over the basal turn scala media was shaved to create a small fenestra through the thinned bone. A glass microelectrode filled with 0.15 M KCl and connected to a direct current amplifier (model KS-700, World Precision Instruments) was passed through the fenestra and into the scala media to record the endocochlear potential. A silver-silver chloride reference wire was placed in the animal's neck musculature.

Ultrastructural Evaluation of the Tmprss3^{Y260X} Mouse Cochlea

Animals were decapitated under deep anesthesia, and their cochleae were prepared using our scanning electron microscopy (SEM) and transmission electron microscopy (TEM) standard protocols (see Ref. 12). For SEM, a total number of 39 mice (1 ear/animal), including eight *Tmprss3*^{WT} and 31 *Tmprss3*^{Y260X} homozygous mice (see Table 1 for details), were used. The surface of the organs of Corti was observed, from the cochlear base to apex, using a Hitachi S4000 electron microscope. For TEM, a total number of 16 mice, including 14 *Tmprss3*^{Y260X} homozygous mice (1 ear/animal taken at 10 days ($n = 1$), 11 days ($n = 5$), 12 days ($n = 5$), 14 days ($n = 1$), 19 days ($n = 1$), and 4 months ($n = 1$)) and two *Tmprss3*^{WT} mice (11 days ($n = 1$) and 19 days ($n = 1$)) were used. Ultrathin radial sections of the organ of Corti, taken at different levels along the cochlear spiral, were observed using a Hitachi 7100 electron microscope. In addition, the cristae ampullares, utricules, and saccules from four 4-month-old *Tmprss3*^{Y260X} homozygous mice were also investigated using TEM. The samples were processed and studied under the same conditions as the cochleae.

Sensory Hair Cell Counting

Quantitative evaluation of sensory hair cell loss was performed using SEM. The mouse cochlea length has been found to average 6 mm (13), including the basal (3 mm), the middle (2 mm), and the apical (1 mm) coils. The number of missing hair cells was counted in six segments of 1 mm each normally containing a mean number of 110 inner hair cells (IHCs) and 125 × 3 outer hair cells (OHCs) per mm. Hair cells were counted as absent if the stereociliary bundles and cuticular plates were missing. Cytocochleograms represent the percentage of missing hair cells in the three rows of OHCs and in the row of IHCs in the basal, middle, and apical regions.

Assessment of Balance Function

Rotarod—The balance and motor coordination of *Tmprss3*^{WT} and *Tmprss3*^{Y260X} homozygous mice were assessed on a rotarod apparatus (Bioseb, Chaville, France). Ten adult mice of each genotype were first given a pretraining trial on day 1 in order to familiarize them with the rotating rod. They were trained to stay on the rod first at the lowest speed (4 rpm) and progressively at higher speeds (up to 10 rpm). They returned to the rotating rod following each fall (total of 4–5 trials on day 1). Testing of the mice occurred on days 2, 3, and 4 at fixed speed (10 rpm), and latency to fall was measured for a maximum of 180 s. Each mouse underwent 4 trials/day; the first one was considered as training trial and the second, third, and fourth ones were recorded. For each day, the data were averaged for each mouse (values from the third and fourth trials) and then averaged for each group (*Tmprss3*^{WT} and *Tmprss3*^{Y260X} homozygous mice).

Behavioral Experiments—The vestibular rating score was estimated as described previously (14, 15). *Tmprss3*^{WT} and *Tmprss3*^{Y260X} mice ($n = 10$ each) were each scored from 0 to 4, corresponding to normal behavior to maximal vestibular deficit. A score of 0 means that behavior is normal; a score of 1 means that the behavior is abnormal, but no specific vestibular deficit is effectively determined; a score of 2 corresponds to an identified but slight vestibular deficit; a score of 3 describes an identified and evident deficit; and a score of 4 means that vestibular deficit is maximal. Seven different tests were sequentially scored and totaled to rate the vestibular deficit as follows. 1) Head bobbing was tested, when abnormal intermittent backward extension of the neck was observed. 2) Circling stereotyped movement was tested, ranging from none to compulsive circles around the animal's hips. 3) Retropulsion, a typical backward walk reflecting vestibular disturbance, was tested. 4) The tail-hanging reflex, which normally induces a normal forelimb extension to reach the ground, results in the ventral bent of the body and grip of the tail when the vestibular deficit is maximal. 5) The contact-inhibition reflex normally leads the animal to hold on to a metal grid in a supine position to return when its back touches the ground. In the case of vestibular deficit with a lack in the body orientation referential, this reflex is abolished, and the animal continues gripping the grid in a supine position. 6) The air-righting reflex is necessary for animals to land on their feet when they fall from a supine position; vestibular dysfunction impairs this normal reversal, and a maximal deficit leads the animal to land on its back when dropped from a height of 40 cm onto a foam cushion. 7) Swimming was tested, ranging from a normal swimming behavior to drowning due to loss of all proprioceptive clues. Scores for all of these tests were totaled to obtain the final vestibular deficit score.

Immunohistochemistry—Animals (20–30 g) were anesthetized with pentobarbital (0.4%) and then decapitated. Temporal bones were dissected out and fixed by immersion with 4% paraformaldehyde in PBS (0.01 M). For adult sensory epithelia, excised whole cristae, utricles, and saccules were preincubated in blocking solution (0.5% fish gelatin, 0.5% Triton X-100, and 1% BSA in PBS) to prevent nonspecific binding. Samples were then incubated with primary anti-myosin VIIa rabbit poly-

clonal antibody (1:300). Secondary antibodies revealed specific labeling with Alexa 647-conjugated donkey anti-rabbit sera (1:200; Molecular Probes, Inc., Eugene, OR) and TRITC-conjugated phalloidin-stained actin (1:200). A Zeiss 5 live duo laser-scanning confocal microscope (RIO Imaging, Montpellier, France) allowed the observation of mounted epithelia on slides. For epithelia of newborn and young animals, the only actin staining was processed and monitored using an apotome microscope (RIO Imaging, Zeiss AxioImager). Adobe Photoshop software was used for final image processing.

Morphometric Analysis—Hair bundles stained for actin were quantified in the stacks of saccules from newborn and young animals using Metamorph imaging software. The number of hair bundles was manually counted and normalized by the area monitored to obtain the density of hair bundles per 100 μm^2 of saccular epithelium.

Statistical Analysis

For the assessment of hearing function, all data are expressed as means ± S.E. To evaluate the significance of the functional difference between *Tmprss3*^{WT} and *Tmprss3*^{Y260X} mice, statistical tests were performed on Sigmaplot 2000 for Windows (version 6.1). All comparisons between means were performed using Student's paired two-tail *t* tests. The data values are expressed as means ± S.E. Density of hair bundles between developing and adult animals was compared using analysis of variance followed by Tukey's test. For vestibular deficit, behavioral score were compared between *Tmprss3*^{WT} and *Tmprss3*^{Y260X} homozygous mice using the Mann-Whitney test. For the rotarod experiment, one sample *t* test was performed.

Cloning of Tmprss3 Long Isoform and Expression in HeLa Cells

Total RNA was isolated from the inner ear of wild type mice and reverse transcribed. The coding regions of the *Tmprss3* long isoform were PCR-amplified and subcloned into the EYFP-N1 vector (Clontech, Mountain View, CA) using TMPRSS3lSal1-S (5′-TTAGTCGACATGGCCGCTTCAGAAATGGTGGAG-3′) and TMPRSS3lBamH1-AS (5′-TTAGGATCCAAAGTCTTCAGATCTCTCTCCAACTG-3′). Plasmid containing the *Tmprss3* short isoform tagged with V5 was described previously (8). Plasmids were transfected into HeLa cells using the Lipofectamine LTX Plus transfection reagent (Invitrogen). The endoplasmic reticulum was labeled with a rabbit anti-calreticulin polyclonal antibody (Stressgen, Ann Arbor, MI) at 1:800. V5 epitope was revealed with a mouse anti-V5 monoclonal antibody (Invitrogen) at 1:1000.

Tissue Expression of Tmprss3a and Tmprss3f

Expression of *TMPRSS3a* and *Tmprss3f* was evaluated using a mouse tissue cDNA panel. Briefly, total RNA was isolated using the RiboPure™ kit (Ambion, Austin, TX) and transformed into cDNAs using the SuperScript™ III first strand synthesis system for RT-PCR (Invitrogen). *TMPRSS3a* cDNA was amplified with primers 5′-AACGCAGAGGATGAGTACCGA-3′ and 5′-AGCAACAGCATCTGCATCTGGT-3′, and *Tmprss3f* was amplified with primers 5′-TATTCCTGCTTCCAAGGATGGC-3′ and 5′-GAGGACATGTTTCCACCCACAA-3′.

Spiral Ganglion Neuron Counting

Cryostat sections of 12 μm were taken throughout the entire cochleae of *Tmprss3*^{WT} ($n = 10$) and *Tmprss3*^{Y260X} homozygous ($n = 10$) mice. To better visualize neurons in the spiral ganglion, the sections were immunolabeled using β III tubulin (type I spiral ganglion neurons, Monoclonal antibody, 1:3000, Covance, Emeryville, CA) and peripherin (type II spiral ganglion neurons, rabbit anti-peripherin polyclonal antibody, 1:400, Chemicon International, Temecula, CA) and visualized using a Zeiss confocal microscope. To avoid counting the same neurons twice, only one section of entire cochlea was used for quantification using ImageJ software. Quantitative data were expressed as the mean number of neurons per 3600 μm^2 ± S.E. Student's *t* test was used for statistical analysis of the data ($p < 0.01$).

RESULTS

Generation of Tmprss3 Mutant Mice; the Tmprss3^{Y260X} Protein-truncating Mutation

The *Tmprss3* gene, which maps on mouse chromosome 17, is composed of 12 coding exons. Mutation screening of the *Tmprss3* gene in the Ingenium Pharmaceuticals G1 mouse DNA archive revealed a T to A substitution in exon 7 (at a position 780 bp from the start codon, NM_024022.2), resulting in a nonsense mutation at amino acid 260 (Y260X) (Fig. 1*A*). This mutation would result in the production of a 194-amino acid truncated protein, deleted of most of its protease domain (Fig. 1*B*).

Sperm from G1 offspring carrying the *Tmprss3*^{Y260X} mutation and C57BL/6 oocytes were used to generate heterozygous hybrid *Tmprss3*^{Y260X} founders via *in vitro* fertilization. These founders were subsequently backcrossed for at least 6 generations to wild type C3HeB/FeJ mice. *Tmprss3*$^{Y260X/+}$ heterozygotes were intercrossed to obtain *Tmprss3*$^{Y260X/Y260X}$ homozygote mice (named *Tmprss3*^{Y260X} for simplicity).

To evaluate the effect of the *Tmprss3*^{Y260X} mutation on RNA processing, total RNA was extracted from various tissues, including inner ear, brain, intestine, skeletal muscle, liver, and kidney of three 4-week-old *Tmprss3*^{Y260X} heterozygous mice. Sequencing chromatograms obtained from RT-PCR products encompassing the Y260X mutation showed clear heterozygosity at the mutated position, suggesting that both *Tmprss3*^{WT} and *Tmprss3*^{Y260X} alleles were expressed in all tissues tested (data not shown). Expression of the *Tmprss3*^{WT} and *Tmprss3*^{Y260X} homozygous mutant protein was studied by Western blots on protein extracts from P60 (Fig. 1*C*) and P10 (Fig. 1*D*) *Tmprss3*^{WT} and *Tmprss3*^{Y260X} homozygous mutant cochleae and HeLa cells transfected with Tmprss3. Several Tmprss3 antibodies were tested, but none proved to specifically detect Tmprss3. The best results were obtained with an antibody raised against the C terminus of Tmprss3 protein and already described by Guipponi *et al.* (9). Although this antibody showed nonspecific binding, the additional bands did not interfere with the detection of Tmprss3. The Tmprss3-Cter antibody revealed a strong 50 kDa band in wild type cochleae and in transfected HeLa cells (star). As expected, the 50 kDa band was absent in *Tmprss3*^{Y260X} homozygous mutant cochleae because

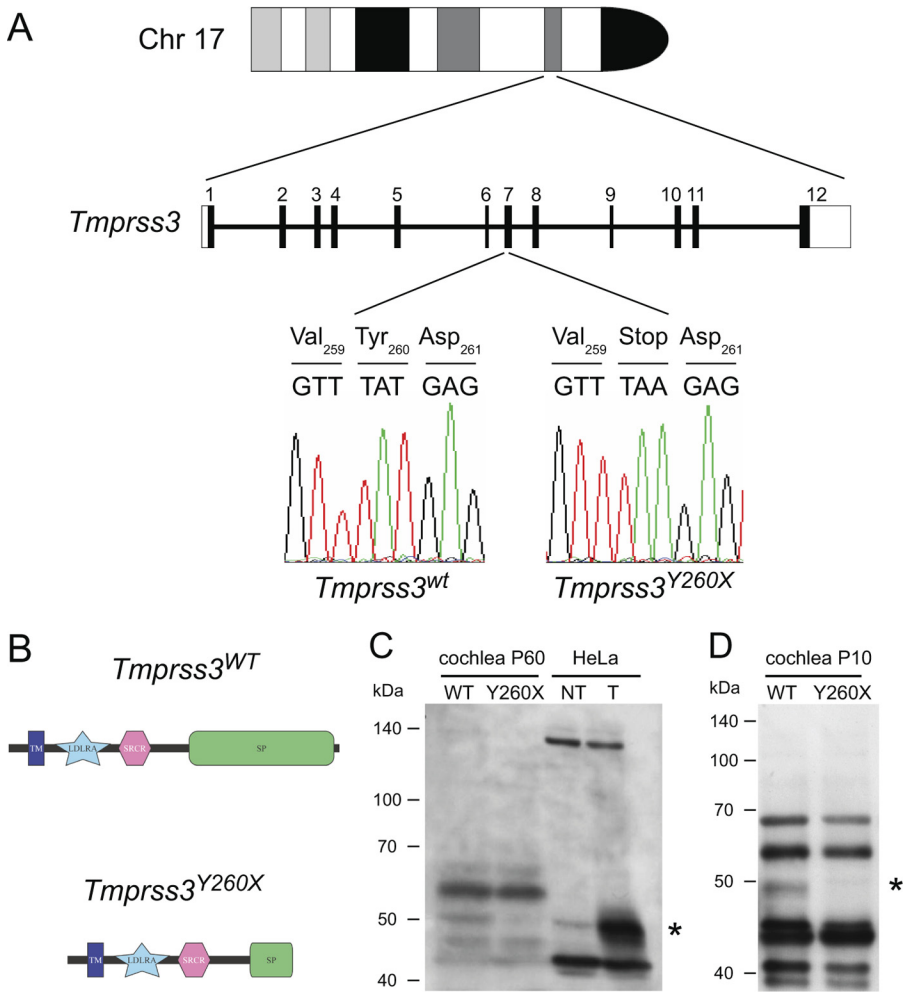

FIGURE 1. **Nonsense mutation in the *Tmprss3* gene.** *A*, the *Tmprss3* gene is located in the A3.3 region of mouse chromosome 17 (*top ideogram*). *Tmprss3* contains 12 exons (*black boxes*). A deoxythymidine nucleotide (*T*) in exon 7 of *Tmprss3*^{WT} (*left chromatogram*) is replaced by a deoxyadenosine (*A*) in the *Tmprss3*^{Y260X} homozygous strain, as shown in the *right chromatogram*. This point mutation changes amino acid 260 of Tmprss3 from tyrosine (*Tyr*) to a stop codon (*Stop*), as shown in the *translation lines*. *B*, the tyrosine to stop amino acid substitution (*Y260X*) is localized to the serine protease domain of Tmprss3. This results in a truncated protein without catalytic activity. Shown are Western blots using the Tmprss3-Cter (*C* and *D*) antibody on mouse *Tmprss3*^{WT} and *Tmprss3*^{Y260X} homozygous cochleae at P60 (*C*) and P10 (*D*) and on non-transfected (*NT*) and transfected (*T*) HeLa homogenates. The Tmprss3-Cter antibody detects a strong overexpressed 50 kDa band (*star*) in the transfected HeLa homogenate with a faint signal in non-transfected HeLa cells, suggesting that Tmprss3 might be faintly expressed in HeLa cells. This band, corresponding to Tmprss3, is also detected in *Tmprss3*^{WT} cochlea extracts and is absent in *Tmprss3*^{Y260X} homozygous cochlea at P60 and P10. In all homogenates, nonspecific bands are also observed.

the epitope used for the C-terminal antibody generation is no longer present in *Tmprss3*^{Y260X} homozygous mutant mice. However, due to the lack of specific N-terminal antibody, this experiment does not allow us to determine if the truncated protein is present or absent. Moreover, because the Tmprss3-Cter antibody cross-reacts with other proteins, we were not able to unequivocally identify the inner ear cells expressing Tmprss3 by immunohistochemistry. Finally, *Tmprss3*^{Y260X} homozygous mutant were born at the expected Mendelian ratio in matings between heterozygous animals and resembled the wild type and heterozygous littermates in viability, growth rate, fertility, and gait.

Tmprss3^{Y260X} *Mutant Mice Are Completely Deaf*

Auditory function was tested in 60-day postnatal mice by recording sound-evoked ABRs. Wild type *Tmprss3*^{WT} ($n = 10$) and *Tmprss3*^{Y260X} heterozygous mice ($n = 10$) showed the classical ABR waveforms (I–IV) in responses to all sound stimulation from 2 to 32 kHz with thresholds between 20 and 45 dB SPL. In contrast, the *Tmprss3*^{Y260X} homozygous ($n = 10$) littermates showed no visible ABRs, even for stimulus intensities above 90 dB SPL (Fig. 2*A*). This analysis was completed by DPOAE recordings, which reflect the activity of OHCs. Consistent with ABR recordings, DPOAEs were not significantly different in wild type *Tmprss3*^{WT} ($n = 10$) and *Tmprss3*^{Y260X} heterozygous mice ($n = 10$), albeit it was absent in *Tmprss3*^{Y260X} homozygous ($n = 10$) littermates at all stimulus frequencies and intensities studied (Fig. 2*B*).

Tmprss3^{Y260X} *Mutant Mice Display Vestibular Deficits*

Several tests aimed at assessing the vestibular functions were performed on *Tmprss3*^{Y260X} homozygous mice (4 months and $n = 10$). Fixed speed rotarod performance, measured as latency to fall, was significantly reduced for mutant mice when compared with wild type littermates (Fig. 2*C*). To further refine the vestibular defects, Tmprss3 mutants were subjected to seven

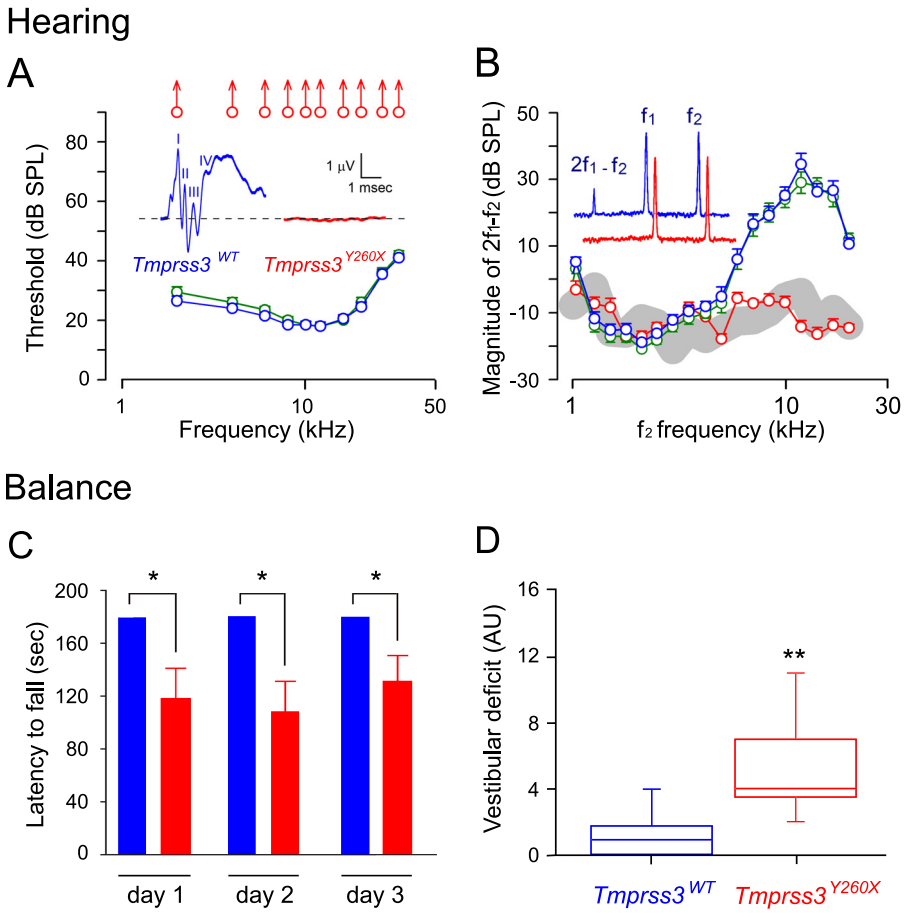

FIGURE 2. **Assessment of hearing and balance impairments in *Tmprss3*^{Y260X} mice.** *A*, mean ABR thresholds (mean ± S.E.) for P60 *Tmprss3*^{WT} (*blue circles*; $n = 10$), P60 *Tmprss3*^{Y260X} heterozygous (*green circles*; $n = 10$) and P60 homozygous mutant (*red circles*; $n = 10$) mice. All *Tmprss3*^{Y260X} homozygous mice displayed no ABR wave, even at the highest intensity tested (100 dB). This is symbolized by an *upward arrow* on *top* of the *red open circle*. *Inset*, representative ABR recordings from *Tmprss3*^{WT} (*left*) and *Tmprss3*^{Y260X} homozygous (*right*) P60 mice at 20–100 dB SPL of pure sound at 8 kHz. No ABR waveform is visible in the *Tmprss3*^{Y260X} homozygous mouse recordings. *B*, recordings of distortion product otoacoustic emissions (2f1 − f2) reflect the cochlear nonlinearity as a result of outer hair cell function. P60 *Tmprss3*^{WT} (*blue circles*; $n = 10$) and P60 *Tmprss3*^{Y260X} heterozygous mice (*green circles*; $n = 10$) have normal otoacoustic emissions, whereas P60 *Tmprss3*^{Y260X} homozygous mice have none (*red circles*; $n = 10$). The background noise level of the recording system in the absence of sound is also depicted (*shadowed area*; $n = 10$). Values are mean ± S.E., and *n* indicates the number of animals tested. *C*, abnormal balance ability in the *Tmprss3*^{Y260X} homozygous mice. Shown is a comparative analysis of the time spent on fixed speed rotating rod (10 rpm) before falling (latency to fall in seconds) for P120 *Tmprss3*^{WT} (*blue*; $n = 10$) and P120 *Tmprss3*^{Y260X} homozygous (*red*; $n = 9$) mice. Each mouse was subjected to 4 trials of 180-s duration. The latency to fall was measured in the third and fourth trials. Data are mean ± S.E. ($n = 10$; *t* test, $p < 0.05$ for the genotype variable). *D*, evaluation of vestibular deficits in P120 *Tmprss3*^{WT} mice (*blue*; $n = 10$) and in P120 *Tmprss3*^{Y260X} homozygous mice (*red*; $n = 9$). Seven different tests were evaluated (scored from 0 to 4) and totaled to obtain the vestibular deficit (in arbitrary units (*AU*)). The position of the median value is shown as the *horizontal line* in the *boxes*. The *bottom* and *top* of this *box* identify the first and third quartiles. The *height* of the *boxes* corresponds to the interquartile range, as the characteristics of the data variability. The *error bars* mark the minimal and maximal non-distant values. *Tmprss3*^{Y260X} homozygous mice display slight but statistically significant vestibular deficits in comparison with wild type mice (**, $p = 0.002$; Mann-Whitney test).

behavioral tests, including the swimming, head bobbing, circling, retropulsion, tail-hang reflex, contact inhibition of the righting reflex, and air-righting reflex tests. These tests showed that *Tmprss3*^{Y260X} homozygous mice, unlike wild type littermates, have an increased latency to return on the contact inhibition reflex, a tendency to swim on the side, and a tendency to occipital landing when landing at the tail-hanging reflex (Fig. 2*D*). Collectively, these tests showed that *Tmprss3*^{Y260X} homozygous mice present a mild but still significant vestibular deficit when compared with their wild type littermates. Overall, these results indicate that the *Tmprss3*^{Y260X} mutation leads in mice to autosomal recessively inherited early onset syndromic deafness.

Deafness Is Due to a Rapid and Massive Degeneration of Hair Cells at the Onset of Hearing

SEM Analysis—The organ of Corti of Tmprss3^{Y260X} homozygous mice (Fig. 3, *A–E*) was investigated using SEM and compared with the organ of Corti of *Tmprss3*^{WT} mice (Fig. 3, *F–J*), from birth to 4 months of age. Both groups of mice essentially showed the same features until 11 days. Then hair cells rapidly disappear in the Tmprss3^{Y260X} homozygous mice, whereas they were preserved in the wild type animals.

In the *Tmprss3*^{Y260X} homozygous mice, at birth, the IHCs and the OHCs showed immature stereociliary bundles all along the cochlea (data not shown). At postnatal day 7 (P7), the stereociliary bundles were well developed on both types of hair cells (Fig. 3*A*). At P11 (Fig. 3*B*), the stereociliary bundles showed an adult-like appearance (almost linear on IHC and W-shaped on OHC). In addition, the thick kinocilium that accompanied the stereociliary bundles during the period of hair cell development had completely regressed on the OHCs. The unusual presence of one or two additional thin and long kinocilia on the OHCs and the IHCs was the only abnormal feature

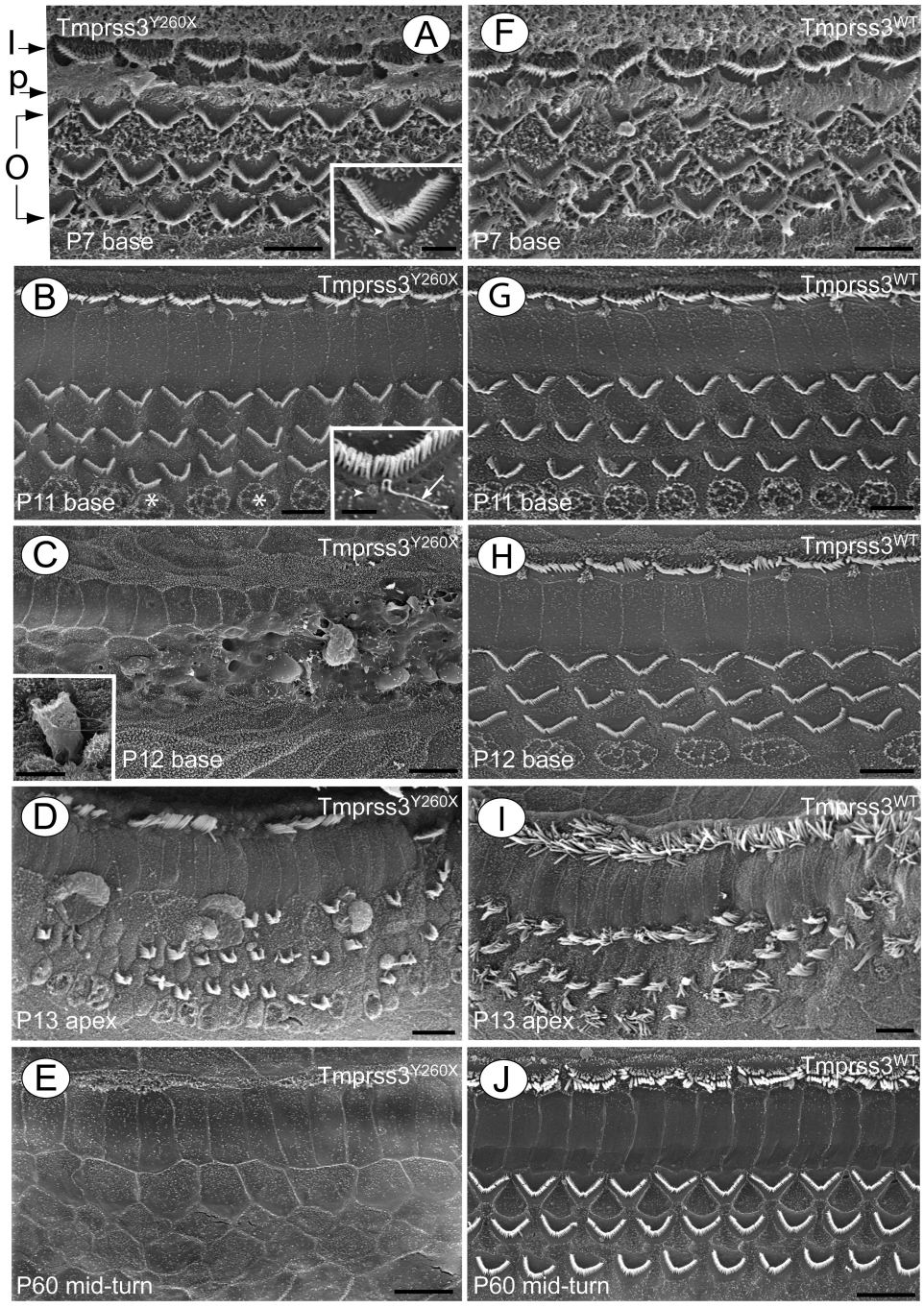

FIGURE 3. **Scanning electron microscopy of the organ of Corti in *Tmprss3*^{Y260X} (*A–E*) and *Tmprss3*^{WT} mice (*F–J*).** *A*, 7 days; basal cochlear region. The stereociliary bundles are already well formed on both the row of IHCs (*I*) and the three rows of OHCs (*O*). Each bundle is associated with a thick kinocilium (see the *inset*). The distance between IHCs and the *first OHC row* is, however, very small because the heads of pillar cells (*p*) are not yet fully developed. The supporting cells are covered with long, densely packed microvilli. *B*, 11 days (basal cochlear region). The surface of the organ of Corti has a mature aspect. The stereociliary bundles are typically organized in one row for IHCs and in three rows for OHCs. Both types of hair cells are separated by the heads of pillar cells. Consistent with this stage of cochlear development, the thick kinocilium has already completely regressed on OHCs. In the *inset*, an OHC shows an additional thin and very long kinocilium (*arrow*) near the footprint of the preexisting thick kinocilium (*arrowhead*). Behind the *last row* of *OHCs*, the footprints of the transient marginal pillars are visible (*asterisks*). *C*, 12 days; basal cochlear region. Both IHCs and OHCs have disappeared. The supporting cells have invaded the area of hair cells to form a scar, but in some places (*right half* of the *picture*), the wound is not completely healed. The *inset* shows an OHC partially extruded from the epithelium. *D*, 13 days; apical cochlear region. Both types of hair cells are missing throughout the cochlea except for some remaining hair cells in the apical extremity. *E*, 2 months; middle cochlear region. The hair cells are missing, and the scarring process is achieved all along the cochleae. *F–J* allow comparison of the organs of Corti in *Tmprss3*^{WT} mice with those of *Tmprss3*^{Y260X} homozygous mice, at the same ages and at the same levels of the cochlear spiral. In the *Tmprss3*^{WT} mice, the organs of Corti have a normal appearance and show all hair cells, whatever the conditions. *F*, 7 days; basal cochlear region. *G*, 11 days; basal cochlear region. *H*, 12 days; basal cochlear region. *I*, 13 days; apical extremity. *J*, 2 months; middle cochlear region. The organ of Corti has an adult-like aspect. The density of microvilli is low. Note the absence of marginal pillar footprints. *Scale bars* (*A–H*), 10 μm; *insets*, 1 μm.

TABLE 1

Quantitative evaluation of hair cell disappearance versus the age of *Tmprss3*^{WT} and *Tmprss3*^{Y260X} homozygous mice

Hair cell counts were performed using scanning electron microscopy. The full length of the cochlea is considered to be 6 mm, containing an approximate number of 660 IHCs and 2250 OHCs.

Age[a]	Missing OHCs and IHCs (%) and number (*n*) of *Tmprss3*^{WT} animals	Missing OHCs and IHCs (%) and number (*n*) of *Tmprss3*^{Y260X} animals	Localization of missing hair cells
days			*mm from base*
0–10	(*n* = 4) OHCs = 0; IHCs = 0	(*n* = 4) OHCs = 0; IHCs = 0	
11	(*n* = 4) OHCs = 0; IHCs = 0	(*n* = 6) OHCs = 0; IHCs = 0	
12	(*n* = 4) OHCs = 0; IHCs = 0	(*n* = 2) OHCs = 0; IHCs = 0	
		(*n* = 1) OHCs = 5; IHCs = 5	0.6–0.9
		(*n* = 1) OHCs = 8,5; IHCs = 8	1–1.5
		(*n* = 2) OHCs = 80; IHCs = 80	0–5
13	(*n* = 4) OHCs = 0; IHCs = 0	(*n* = 1) OHCs = 0; IHCs = 0	
		(*n* = 1) OHCs = 80; IHCs = 84	0–5
		(*n* = 1) OHCs = 97; IHCs = 95	0–5.82
		(*n* = 1) OHCs = 90; IHCs = 90	0–5.40
		(*n* = 2) OHCs = 100; IHCs = 100	
14	(*n* = 4) OHCs = 0; IHCs = 0	(*n* = 2) OHCs = 97; IHCs = 98	0–5.88
		(*n* = 1) OHCs = 100; IHCs = 100	0–6
≥15	(*n* = 4) OHCs < 1; IHCs < 1	(*n* = 6) OHCs = 100; IHCs = 100	0–6

[a] Age is given in postnatal days.

seen in some cochleae (one cochlea of two at P7 and two of six at P11) of *Tmprss3*^{Y260X} homozygous mice (Fig. 3, *B* and *inset*) from birth to 11 days. These atypical structures were generally located near the thick kinocilium (or its footprint), although they could be seen in other parts of the cuticular plates.

A prominent finding observed in the *Tmprss3*^{Y260X} homozygous mice was the abrupt occurrence of massive hair cell loss from day 12 onward (Table 1 and Fig. 3, *C–E*). At P12, four animals among six *Tmprss3*^{Y260X} homozygous mice actually suffered hair cell loss. In two of these mice, missing IHCs and OHCs (Fig. 3*C*, *inset*) were observed in limited segments of the basal cochlear region (0.6–0.9 and 1–1.5 mm from the basal extremity, respectively), the more apical parts of these cochleae being preserved (data not shown). The two other animals showed complete loss of IHCs and OHCs all along the basal and middle cochlear regions (*i.e.* the 5 mm starting from the basal extremity; Table 1). Strikingly, in these four specimens, both types of hair cells seemed to have disappeared simultaneously. At P13, two of six *Tmprss3*^{Y260X} homozygous mice showed complete (100%) hair cell loss. Three mutant mice showed severe (80–90%) loss of hair cells with only a few remaining hair cells in the last apical 150–200 μm (Fig. 3*D*). A single mutant mouse did not show any signs of cochlear defect. At P14 onwards (Fig. 3*E*), all *Tmprss3*^{Y260X} homozygous mice ($n = 3$ at P14 and $n = 6$ at $p \geq 15$) showed complete hair cell loss along the length of the cochlear duct.

All *Tmprss3*^{WT} mice investigated from birth to 4 months ($n = 24$) showed a full contingent of hair cells throughout the cochleae (Table 1 and Fig. 3, *F–J*), although a few scattered hair cells (<1% total hair cells; Table 1) were occasionally missing (Fig. 3*J*) in the cochleae of the oldest animals (2 and 4 months). Additional thin kinocilia were not seen on hair cells in wild type mice.

Ultratructural Analysis Using TEM—In 11-day-old Tmprss3^{Y260X} homozygous mice, the organ of Corti was almost mature (Fig. 4A). The tunnel of Corti and the spaces of Nuel were widely opened, and both IHCs and OHCs showed well formed stereocilia, including the tip links involved in the transduction process (Fig. 4*A* and *upper inset*). Afferent synapses were evidenced at the basal pole of the IHCs (Fig. 4*B*). Medial efferent synapses were already formed at the basal pole of OHCs, and small afferent buttons were also contacting the hair cells (Fig. 4*C*). The spiral lamina contained densely packed myelinated nerve fibers (Fig. 4*A*, *lower inset*).

Consistent with our SEM data, the organ of Corti of *Tmprss3*^{Y260X} homozygous mice was profoundly altered in the basal and middle cochlear turns at postnatal day 12 (Fig. 4*D*). Both IHCs and OHCs were absent or disappearing, and the tunnel of Corti and the spaces of Nuel were collapsed. Pieces of hair cells extruded from the epithelium were seen in the endolymphatic compartment (Fig. 4*E*), whereas remnants of hair cells (Fig. 4*F*) were seen in the scarring epithelium. In 4.5-month-old *Tmprss3*^{Y260X} homozygous mice, the organ of Corti has completely regressed in the basal cochlear turn, where a single layer of undifferentiated epithelial cells remained. The more apical regions showed a scarred epithelium in which pillar cells were still recognizable (not shown).

Qualitative and Quantitative Analysis of Spiral Ganglion Neurons in Tmprss3^{Y260X}

In 12- and 14-day old *Tmprss3*^{Y260X} homozygous mice, the ganglion neurons and their associated glial cells had a healthy appearance (supplemental Fig. S1*A*). In contrast, at 4 months of age, loss of ganglion neurons had occurred, and the remaining ones showed several abnormalities, including retraction of the cell body, deformation of their nucleus, and disorganization of the myelin envelope (supplemental Fig. S1*B*). Determination of the time course of ganglion neuron loss revealed that type I ganglion neuron density is similar in the basal and medial turns of the cochlea in wild type and Tmprss3 mutant mice until P90. Neuronal loss was evident at P180 and P365, with mutant mice displaying a much reduced density of type I neurons when compared with wild type animals (supplemental Fig. S1*C*).

Deafness Is Not Due to a Defect in the Stria Vascularis Function

TEM analysis revealed that the stria vascularis of both control and mutant mice displayed a typical appearance, with numerous blood vessels and prominent basolateral infoldings of the marginal cells interlacing with intermediate cell digita-

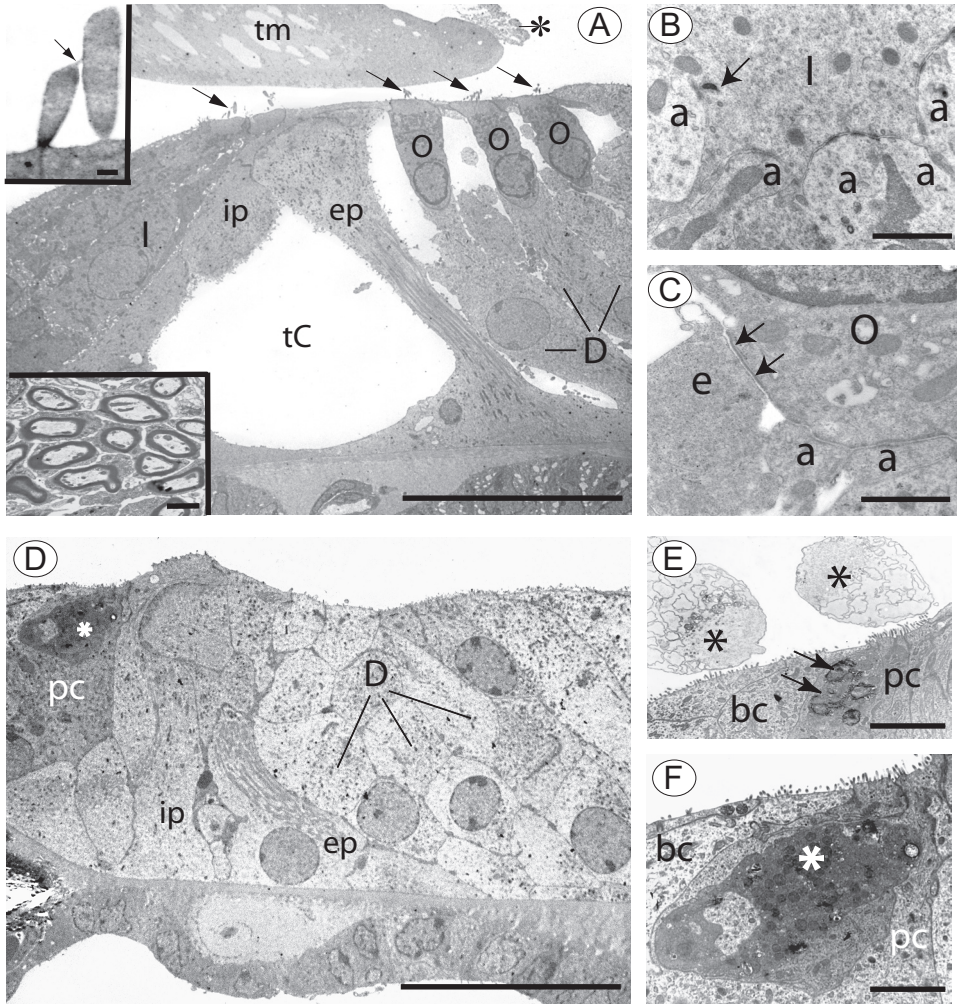

FIGURE 4. **Transmission electron microscopy of the organ of Corti in *Tmprss3*^{Y260X} mice.** *A–C*, 11 days. *A*, upper basal region of the cochlea. The IHCs (*I*) and OHCs (*O*) are present and have a normal appearance. Their stereocilia (*arrows*) are well erected, and tip links are distinguishable (*arrowhead* in the *upper inset*). The tunnel of Corti (*tC*) and the spaces of Nuel around the OHCs are well opened. Numerous myelinated nerve fibers (*lower inset*) are present in the spiral lamina. Note the piece of a marginal pillar attached to the distal part of the tectorial membrane (*asterisk*). *D*, Deiters cells; *ip*, inner pillar cell; *ep*, external pillar cell; *tm*, tectorial membrane. *B*, basal pole of an IHC (*I*) contacted by several (radial) afferent endings (*a*). A synaptic ribbon (*arrow*) is present within the IHC, facing an afferent. *C*, basal pole of an OHC in contact with two (spiral) afferent endings and one larger efferent terminal (*e*). The *arrows* point to a postsynaptic cistern within the OHC. *D–F*, 12 days; middle cochlear region. *D*, the hair cells have disappeared from the epithelium and are replaced by extensions of Deiters cells in the OHC area and by inner supporting cells, including phalangeal cells (*pc*), in the IHC area. The external and inner pillar cells are collapsed. The tectorial membrane (not seen on the picture) has a normal appearance. *E*, in the IHC region, corpses of hair cells (*asterisks*) have been extruded from the epithelium into the endolymphatic space (border cells (*bc*)). The *arrows* point to cellular debris within the cytoplasm of a phalangeal cell. *F*, enlargement of a damaged IHC remnant (*asterisk*) seen in *D*. The IHC remnant is wrapped by a phalangeal cell and shows dark mitochondria and a dense cytoplasm. *Scale bars*, 10 μm (*A* and *D*) and 1 μm (*B*, *C*, *E*, *F*, and *lower inset* in *A*), and 0.1 μm (*upper inset* in *A*).

tions and normal basal cells (supplemental Fig. S2, *A* and *B*). The only change observed in *Tmprss3*^{Y260X} homozygous mice was a slight swelling of intercellular spaces between the marginal and intermediate cells (supplemental Fig. S2*B*, *arrow*). The proper functioning of the stria vascularis was assessed by recording the EP in adult (P60) *Tmprss3*^{WT} and *Tmprss3*^{Y260X} homozygous mice. Both wild type and mutant mice showed normal values, suggesting normal physiology of the stria vascularis (*Tmprss3*^{WT} = +101.6 ± 5.9 mV and *Tmprss3*^{Y260X} homozygous = +106.3 ± 4.7 mV; $p = 0.83$) (supplemental Fig. S2*C*).

Saccular Hair Cells Are Selectively Lacking in Tmprss3^{Y260X} *Mice*

The general histology of *Tmprss3*^{Y260X} homozygous mouse cristae (Fig. 5, *A* and *B*) and utricles (Fig. 5, *C* and *D*) displayed no abnormality. In these epithelia, hair cells (*stars*) and supporting cells (*arrowheads*) were organized similarly to the wild type. Similarly to wild type, tight junctions were present at the apex of these two cell types, whereas hair cells were polarized with their nuclei located above the nuclei of supporting cells, which lined the basal part of the epithelia. Higher magnification observations (Fig. 5, *B* and *D*) confirmed the presence in these sensory epithelia of the two hair cell types that could be identified by characteristic feature: pear shape and calyx-type afferent for type I hair cells; cylindrical shape and bouton afferents for type II hair cells.

Conversely, saccular epithelia (Fig. 5, *E* and *F*) displayed abnormal cell composition and organization. Epithelia were thinner with most hair cells lacking, although supporting cells looked normal. At higher magnification (Fig. 5*F*), no calyx were observed, although some large afferent terminals were present

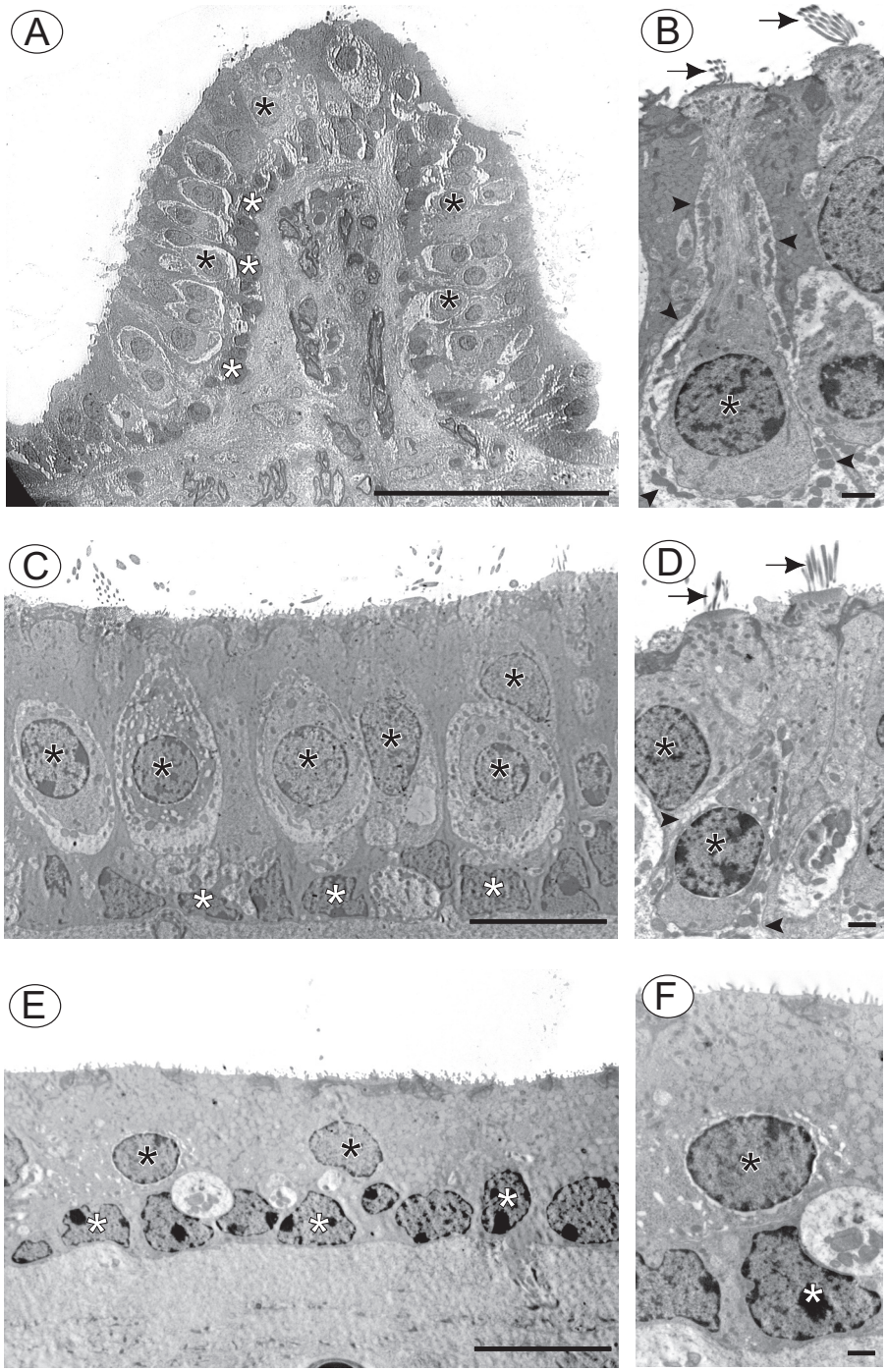

FIGURE 5. **Transmission electron microscopy of vestibular end organs in 4-month-old *Tmprss3*^{Y260X} mice.** *A* and *B*, transverse section of crista. *A*, typical cytoarchitectural organization with both types of hair cells (*black asterisks*), type I and type II, lying on a layer of supporting cells (*white asterisks*). *B*, hair bundles (*arrows*) normally located at the top of hair cells above their cuticular plates. Type I hair cells (*black asterisk*) are recognizable by their typical afferent innervation, the calyx terminal (*arrowheads*) wrapping the basal part of the hair cell body. Nuclei of type II hair cells (*upper right*) are normally located higher in the epithelium. *C* and *D*, transverse section of utricule. *C*, organization of hair cells (*black asterisks*) and supporting cells (*white asterisks*) are also normally preserved in utricules. *D*, *arrows* point to hair bundles overhanging the two types of vestibular hair cells, type I (*left black asterisk*) and its typical calyx afferent (*arrowheads*) and type II (*right black asterisk*). *E* and *F*, transverse section of saccule. *E*, a few unidentified sensory cells (*black asterisk*) still lie on the layer of supporting cells (*white asterisks*) composing a thin epithelia penetrated by an undetermined type of afferents. Hair bundles are no longer observed in this section. *F*, at higher magnification, the sensory cell type (*black asterisk*) and the neighboring afferent terminal are still undetermined. *Scale bars*, 50 μm (*A*), 10 μm (*C* and *E*), and 1 μm (*B*, *D*, and *F*).

within the epithelium, close to unidentified sensory-like cells with no hair bundle.

In adult *Tmprss3*^{Y260X} homozygous mice (more than 4 months old), immunostaining of vestibular hair cells with myosin VIIa and actin fluorescent labeling of their hair bundles confirmed the normal organization of the sensory epithelia in both cristae and utricles (supplemental Fig. S3, *A* and *B*), whereas it was severely altered in saccules (supplemental Fig. S3*C*). The lack of saccular hair cells was common to all *Tmprss3*^{Y260X} homozygous mice analyzed ($n = 3$ males and $n = 3$ females).

TABLE 2
Hair bundle density in saccular epithelium of developing and adult *Tmprss3*^{WT} and *Tmprss3*^{Y260X} homozygous mice

Age[a]	Number of animals	*Tmprss3*^{WT} hair bundle density	Number of animals	*Tmprss3*^{Y260X} hair bundle density
days		*bundles/100 μm²*		*bundles/100 μm²*
0	3	1.01 ± 0.08	3	0.69 ± 0.04
7	3	0.75 ± 0.05	3	0.87 ± 0.03
10	3	1.03 ± 0.15	3	0.91 ± 0.02
27	3	1.13 ± 0.02	3	0.94 ± 0.10
Adult (>4 months)	3	1.35 ± 0.05[b]	3	0.20 ± 0.08[c]

[a] Age is given in postnatal days.
[b] Data from Ref. 32.
[c] $p < 0.001$.

Fluorescent phalloidin that stains actin filaments was used to highlight and quantify the hair bundles in the sacculus of *Tmprss3*^{Y260X} homozygous mice at different postnatal days (P0, P7, P10, and P27) and in adults (supplemental Fig. S3*D*). Between P0 and P10, when vestibular reflexes involved in balance are becoming established (onset of the vestibular behavior), no difference in the number of hair bundles could be quantified over time or in comparison with the *Tmprss3*^{WT} mice (analysis of variance and *t* test) (Table 2). No statistical difference in the density of hair bundles was seen in P27 saccular hair cells of *Tmprss3*^{Y260X} homozygous mice compared with control mice (Table 2). Conversely, the density of hair cells was drastically and significantly reduced in the saccule of adult (>4 months) *Tmprss3*^{Y260X} homozygous mice (Table 2). The observed time course of the selective saccular hair cells loss indicates that it relies on a progressive degenerative process following the functional activation of the hair cells.

Tmprss3 Is Expressed in Hair Cells

By *in situ* hybridization, we analyzed *Tmprss3* expression in the developing inner ear at P7 and P11. At P7, cochlear and vestibular hair cells (*HC*) were strongly positive for *Tmprss3* (Fig. 6, *A–D*); no signal was observed with a control peripherin probe, except in the type II neurons in the cochlea (*arrowheads*) (Fig. 6*I*). In addition, labeling was observed in the supporting cells of the organ of Corti (*OC*) as well as epithelial cells of the inner (*ISS*) and outer (*OSS*) spiral sulcus. Finally, expression was observed in interdental cells (*IC*) and at a lesser level in the spiral ganglion cells (*SG*). By P11, staining was still observed in the same cochlear and vestibular cells (Fig. 6, *E–H*), whereas no signal was detected with peripherin control probe, except in the type II neurons in the cochlea (*arrowheads*) (Fig. 6*J*).

A Novel Tmprss3 Isoform Is Expressed in the Mouse Inner Ear, Tmprss3f

The *TMPRSS3* gene has been shown to express several alternative transcripts. These transcripts are predicted to encode for proteins of different sizes that mainly vary in their N terminus (1, 16). Recently, a novel *Tmprss3* isoform has been deposited in the GenBank™ nucleotide sequence data base under accession number NM_001163776. This novel mouse *Tmprss3* mRNA (named *Tmprss3f* in this paper) is predicted to produce a protein with 22 additional amino acids at the N terminus (Fig. 7) in comparison with the first described isoform, *Tmprss3a* (NM_024022.2). These additional residues do not seem to encode for any known functional protein domain, like signal peptides. Because *Tmprss3a* does not possess an N-terminal signal peptide, it is expected that these additional amino acids will not affect the expression of the protein. We showed that this novel Tmprss3 isoform may also be present in humans because nucleotide sequence alignment analysis using BLAT (see the UCSC Genome Bioinformatics Web site) revealed the existence of a putative novel human *TMPRSS3* exon that shows significant homology to the novel mouse isoform (supplemental Fig. S4). Similarity between human and mice sequences was 94%, and homology was 89% (supplemental Fig. S5).

Tissue Expression and Subcellular Localization of Tmprss3f

To investigate whether *Tmprss3f* exerts different functions than *Tmprss3a*, we analyzed its expression profile and subcellular localization. RT-PCRs were carried out on mouse P17 tissues (liver, cochlea, retina, brain, cerebellum, spleen, kidney, lung, heart, and muscle). Interestingly, *Tmprss3a* and *Tmprss3f* showed distinct expression pattern. *Tmprss3a* was strongly expressed in liver, cochlea, brain, cerebellum, spleen, lung, and muscle and at a lower degree in retina, kidney, and heart (Fig. 8*A*, *middle*), whereas *Tmprss3f* was strongly expressed only in the cochlea with very faint expression in the cerebellum, spleen, and muscle (Fig. 8*A*, *top*).

Finally, to determine if these two isoforms are differentially localized within the cell, tagged and wild type *Tmprss3f* and *Tmprss3a* proteins were transfected in HeLa cells. Both the short and the long *Tmprss3* isoforms were found to colocalize with the ER marker calreticulin (Fig. 8, *B* and *C*). To ensure that this ER expression is not due to an overexpression artifact, the experiment was replicated without permeabilizing the cells. No labeling was observed at the plasma membrane (data not shown), suggesting that Tmprss3 is really localized in the ER. This novel *Tmprss3* isoform could play a unique role in the cochlea. Indeed, the long N-terminal tail of *Tmprss3f* might be necessary for its targeting to specific ER or plasma membrane microdomains, where it could interact with different signaling molecules in a cell-specific manner.

DISCUSSION

Mutations in the *TMPRSS3* gene cause non-syndromic autosomal recessive deafness (DFNB8/10). In order to explore the physiopathology of *TMPRSS3*-related deafness, we have generated a mouse mutant carrying a nonsense mutation in *Tmprss3* (*Tmprss3*^{Y260X}) that results in the deletion of most of the catalytic domain. This *Tmprss3*^{Y260X} homozygous mutation leads to syndromic autosomal recessive profound hearing loss in

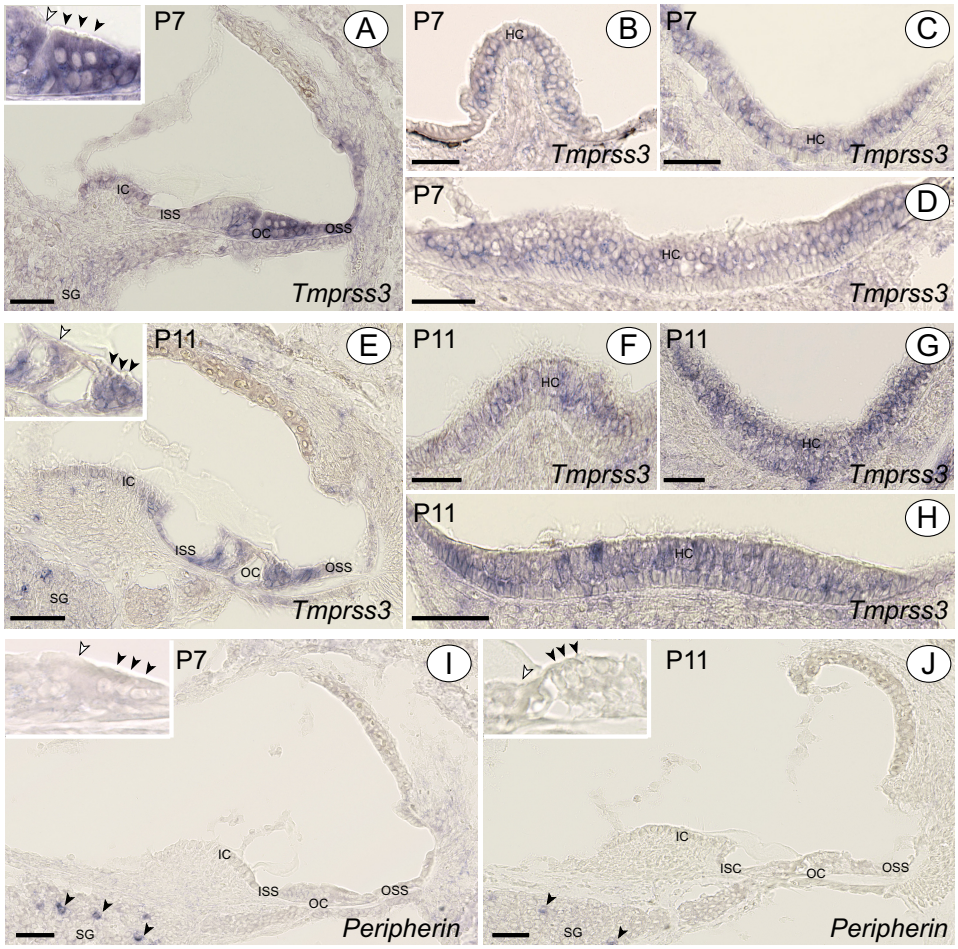

FIGURE 6. **Analysis of *Tmprss3* inner ear expression by *in situ* hybridization.** *A–D*, at P7, Tmprss3 was detected in cochlear hair cells (*A*) and in the crista (*B*), saccular (*C*), and utricular hair cells (*HC*) (*D*). *Inset*, IHCs (*white arrowhead*) and OHCs (*black arrowheads*) were stained at all apico-basal levels of the cochlea. In addition, labeling was observed in supporting cells of the organ of Corti (*OC*), in the inner (*ISS*) and outer (*OSS*) spiral sulcus epithelial cells, as well as in the interdental cells (*IC*). Finally, some spiral ganglion cells (*SG*) were faintly labeled. As a negative control, a peripherin probe was used; no signal was detected in the hair cells (*I*) or in the other cells. Only type II spiral ganglion cells were stained (*arrowheads*). *E–H*, at P11, the same labeling as P7 was observed in the cochlea (*E*) and in the crista (*F*), saccule (*G*), and utricule (*H*). The negative peripherin probe only labels the type II spiral ganglion neurons (*J*).

MAASEMVEVEPEPNIRGPEIVTMGENDPPAAEAPFSFRSLFGLDDLKISPVAPDGDAVAAQILSLLPLKFFPIIV
IGIIALILALAIGLGIHFDCSGKYRCHSSFKCIELTARCDGVSDCKNAEDEYRCVRVSGQRAALQVFTAAAWRTM
CSDDWKSHYAKIACAQLGFPSYVSSDHLRVDALEEQFQGDFVSINHLLSDDKVTALHHSVYMREGCTSGHVVTLK
CSACGTRTGYSPRIVGGNMSSLTQWPWQVSLQFQGYHLCGGSIITPLWIVTAAHCVYDLYHPKSWTVQVGLVSLM
DSPVPSHLVEKIIYHSKYKPKRLGNDIALMKLSEPLTFDETIQPICLPNSEENFPDGKLCWTSGWGATEDGGDAS
PVLNHAAVPLISNKICNHRDVYGGIISPSMLCAGYLKGGVDSCQGDSGGPLVCQERRLWKLVGATSFGIGCAEVN
KPGVYTRITSFLDWIHEQLERDLKT*

FIGURE 7. **Sequence of the novel mouse *Tmprss3f* long isoform.** The 22 novel amino acids are depicted in *red*. No novel functional domain is detected.

mice associated with a mild vestibular deficit. Combined morphological and functional investigations revealed a rapid and massive degeneration of all auditory hair cells beginning at the onset of hearing associated with a significant progressive loss of spiral ganglion neurons starting after P90. The structure and function of the stria vascularis appeared normal. In the vestibular end organs, hair cell loss was restricted to the saccular epithelium and was identifiable only in adult mice. These pathological manifestations provide a clear cellular explanation for the profound hearing loss of *Tmprss3*^{Y260X} homozygous mice and its associated vestibular syndrome. The pattern of cochlear hair cell degeneration was quite unique because the full contingent of hair cell disappeared within 2 days (*i.e.* between P12 and P14, a period that in mice closely corresponds to the onset of hearing) (for a review, see Ref. 17) when measured using compound action potential. In our experiment, no ABRs could be recorded from the earliest analyzed stage (P14). In addition, contrasting with what occurs after ototoxic drug application or noise exposure (see, among others, Refs. 18 and 19), inner and outer hair cells degenerated simultaneously in the *Tmprss3* mutant. These results suggest that the function of Tmprss3 is a *sine qua non* necessity for IHC and OHC sensory activity.

As revealed by scanning and transmission electron microscopic analysis, it is unlikely that *Tmprss3* plays a critical role in the molecular pathways involved in determination or initial differentiation of inner ear hair cells. First, all cochlear hair cells appeared to be present and morphologically normal in *Tmprss3*^{Y260X} homozygous mice at early postnatal stages (until

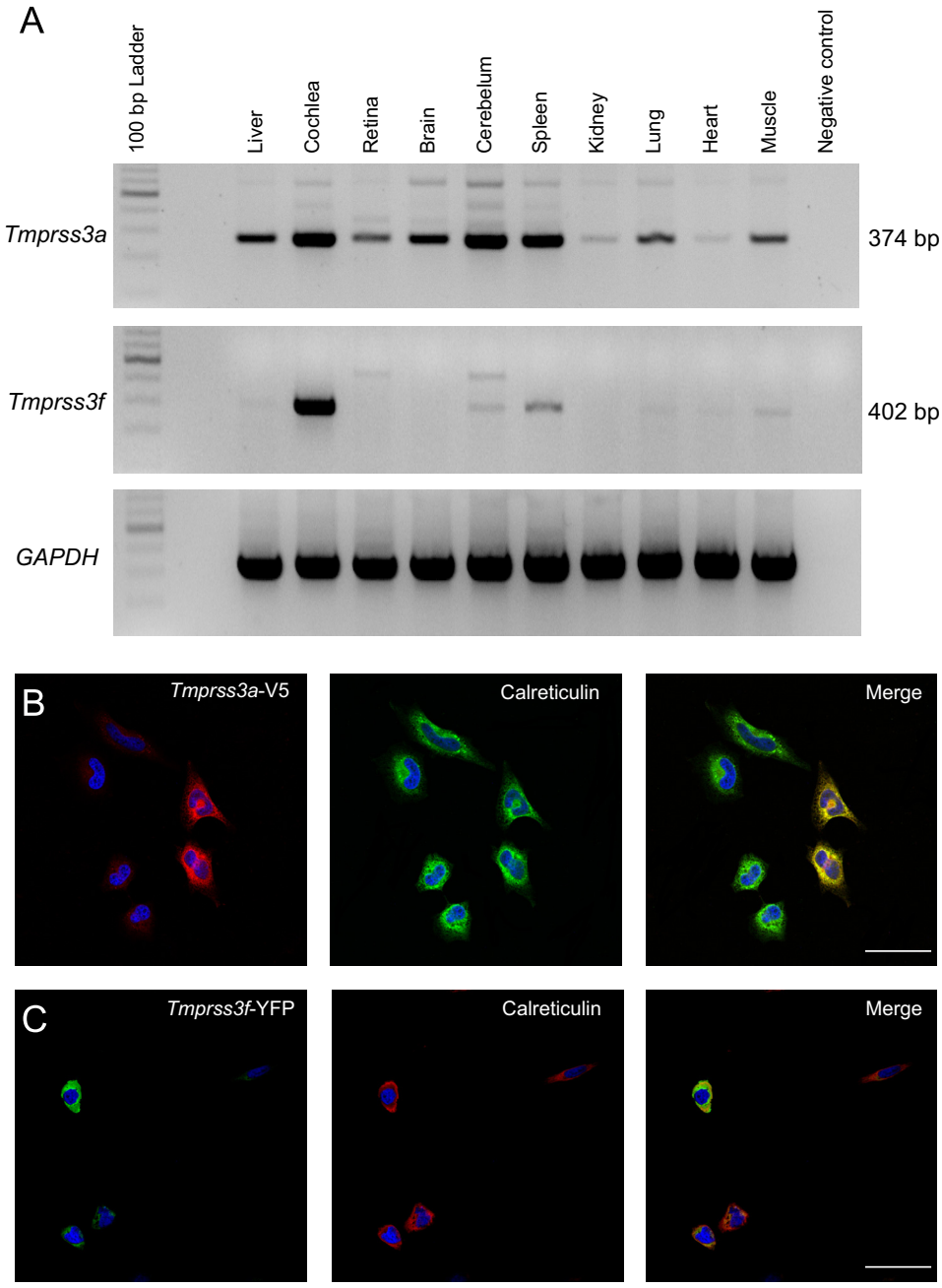

FIGURE 8. **Tissue and subcellular expression of *Tmprss3a* and *Tmprss3f*.** *A*, RT-PCR specific to the *Tmprss3a* and *Tmprss3f* transcripts was performed on cDNA from 10 mouse tissues, which included liver, cochlea, retina, brain, cerebellum, spleen, kidney, lung, heart, and muscle, as indicated. All tissues demonstrated expression of *Tmprss3a* (*top*). In contrast, only cochlea and to a much lower extent cerebellum, spleen, and muscle demonstrated *Tmprss3f* expression (*middle*). *GAPDH* was used as a positive control (*bottom*). The mouse *Tmprss3* cDNAs were cloned into pcDNA3-V5 (*Tmprss3a*) or pYFP-N1 (*Tmprss3f*) expression vectors and transiently transfected in HeLa cells. *B*, Tmprss3a-V5 (*red*) co-localizes with calreticulin (*green*), a marker of endoplasmic reticulum. *C*, Tmprss3f-YFP long form (*green*) co-localizes with calreticulin (*red*). No labeling differences were seen between the short and the long isoforms. *Scale bars*, 50 μm.

P12). However, these cochlear hair cells may have an apparent normal morphology but may not be functionally mature. The ensuing brutal loss of these hair cells at P12, suggests that Tmprss3 play an essential role in the functional maturation of cochlear hair cells. At this time actually, improvement of mechanical properties of the organ of Corti promotes hair cell sensitivity (20). In addition, the fact that both inner and outer hair cells degenerate following the same pattern suggests that at least some signaling pathways controlled by Tmprss3 proteolytic cleavage are common and equally important in both hair cell types.

Regarding the vestibule, selective lack of saccular hair cells in $Tmprss3^{Y260X}$ homozygous mice causes only a mild behavioral deficit, suggesting that other normal sensory epithelia (cristae and utricule) and probably also the vision and the CNS, as suggested in another mouse mutant, were able to partially compensate for saccular dysfunction (21). A normal number of saccular hair cells was counted in P0 $Tmprss3^{Y260X}$ homozygous mice, when mechanotransduction channels are opened in vestibular hair cells (22), and no signs of hair cells loss were evident during the first postnatal days at the setup of endolymphatic composition and onset of vestibular reflexes. The partial and

progressive degeneration of saccular hair cells occurred during adulthood, when saccular function is well established. These results showed that Tmprss3 is not required for saccular hair cell development and activation but seems critical for maintenance of hair cells in adult mice.

It is interesting to note that Tmprrs3 is not necessary for the proper development of both cochlear and saccular hair cells because these hair cells develop normally in mutant mice, and therefore we can postulate that Tmprss3 is not involved in signaling pathways that mediate developmental and specialization processes. Tmprss3 rather acts as a maintenance factor for cochlear and saccular hair cell function and/or survival.

Three recent *in vitro* studies have shown that pathogenic *TMPRSS3* mutations could exert their deleterious effect at the molecular and cellular level through disruption of TMPRSS3 proteolytic activity (3, 9, 23). Therefore, identification of the substrate of TMPRSS3 could facilitate our understanding of the role of TMPRSS3 in hearing. Until now, the ENaC sodium channel has been the only candidate substrate of TMPRSS3 in the inner ear (9). *In vitro* studies using *Xenopus* oocytes have shown that TMPRSS3 proteolytic activity is associated with increased ENaC mediated currents. The ENaC channel is composed of three subunits (α, β, γ), which are all expressed in the cochlea (24, 25) and could participate in the reabsorption of sodium from the endolymph and therefore in maintaining the low sodium concentration in the endolymph (26). However, the TMPRSS3/ENaC functional hypothesis has been challenged by the fact that pseudohypoaldosteronism type 1 patients, who are homozygous for mutations in the ENaC α subunit, exhibit normal hearing (10). In the present study, we showed that the absence of TMPRSS3 proteolytic activity did not affect stria vascularis function, as evaluated by EP recordings. Put together, these data suggest that the mechanism of TMPRRS3 pathogenicity is unlikely to be mediated through ENaC misregulation and, in a more general aspect, via alteration of stria vascularis function.

Tmprss3 belongs to the hepsin/TMPRSS subfamily of type II transmembrane serine proteases which contains seven members. Besides Tmprss3, another member of this subfamily (Tmprss1) has been found to be important for normal hearing (27). Severe hearing impairment in *Tmprss1*$^{-/-}$ mice is accompanied by modest structural defects. Apart from the abnormal tectorial membrane, the other structures of the cochlea appeared to develop properly. These differences in cochlear phenotype in these two mouse mutants indicate that both genes make a unique contribution to inner ear function and suggest interaction with different substrates.

The N-terminal and transmembrane domains, which are two defining features of type II transmembrane serine proteases, are thought to contribute to the targeting of the type II transmembrane serine proteases to the plasma membrane (28). However, Tmprss3 subcellular localization, previously determined using various transfected cell lines appears to be invariably restricted to the endoplasmic reticulum (8, 9). In addition, when transfected cells were treated with the protein synthesis inhibitor, cyclohexamide, expression of Tmprss3 was still visible in the ER. This indicates that this protease is stably anchored in this cellular compartment (8). Interestingly, using a similar approach Tmprss5, Tmprss6, Matriptase-2, and DESC4 expression was clearly seen at the plasma membrane (8, 29–31), suggesting that the ER expression of Tmprss3 is unlikely to be an artifact of the method used. Altogether, these data suggest that Tmprss3 is primarily located in the endoplasmic reticulum membranes, where it might exert its function. However, at this stage, the possibility that upon stimulation, a fraction of Tmprss3 might be translocated to the plasma membrane cannot be ruled out.

The *Tmprss3*^{Y260X} homozygous mice display unique features, including abrupt and concomitant degeneration of inner and outer hair cells by the time of hearing onset. These characteristics may reflect a crucial role for Tmprss3 in the final steps of hair cell morphological/functional maturation. Without any doubt, the characterization of the cochlear substrate repertoire of Tmprss3 will provide significant insights into its role in the hearing process.

Acknowledgments—We thank the Cellular Imaging Facility and the Animal Facility of the Institut des Neurosciences de Montpellier. All of the electron microscopic analyses were performed at the "Centre de Ressources en Imagerie Cellulaire" (Montpellier, France) with the assistance of Chantal Cazevieille. We thank Cécile Delettre for the gift of the different tissue mRNA for the RT-PCR experiment. We especially thank the entire team of the animal facility that took care of the mice.

REFERENCES

1. Scott, H. S., Kudoh, J., Wattenhofer, M., Shibuya, K., Berry, A., Chrast, R., Guipponi, M., Wang, J., Kawasaki, K., Asakawa, S., Minoshima, S., Younus, F., Mehdi, S. Q., Radhakrishna, U., Papasavvas, M. P., Gehrig, C., Rossier, C., Korostishevsky, M., Gal, A., Shimizu, N., Bonne-Tamir, B., and Antonarakis, S. E. (2001) *Nat. Genet.* **27,** 59–63
2. Masmoudi, S., Antonarakis, S. E., Schwede, T., Ghorbel, A. M., Gratri, M., Pappasavas, M. P., Drira, M., Elgaied-Boulila, A., Wattenhofer, M., Rossier, C., Scott, H. S., Ayadi, H., and Guipponi, M. (2001) *Hum. Mutat.* **18,** 101–108
3. Wattenhofer, M., Sahin-Calapoglu, N., Andreasen, D., Kalay, E., Caylan, R., Braillard, B., Fowler-Jaeger, N., Reymond, A., Rossier, B. C., Karaguzel, A., and Antonarakis, S. E. (2005) *Hum. Genet.* **117,** 528–535
4. van Driel, I. R., Goldstein, J. L., Südhof, T. C., and Brown, M. S. (1987) *J. Biol. Chem.* **262,** 17443–17449
5. Südhof, T. C., Goldstein, J. L., Brown, M. S., and Russell, D. W. (1985) *Science* **228,** 815–822
6. Sarrias, M. R., Grønlund, J., Padilla, O., Madsen, J., Holmskov, U., and Lozano, F. (2004) *Crit. Rev. Immunol.* **24,** 1–37
7. Rawlings, N. D., Barrett, A. J., and Bateman, A. (2010) *Nucleic Acids Res.* **38,** D227–D233
8. Guipponi, M., Toh, M. Y., Tan, J., Park, D., Hanson, K., Ballana, E., Kwong, D., Cannon, P. Z., Wu, Q., Gout, A., Delorenzi, M., Speed, T. P., Smith, R. J., Dahl, H. H., Petersen, M., Teasdale, R. D., Estivill, X., Park, W. J., and Scott, H. S. (2008) *Hum. Mutat.* **29,** 130–141
9. Guipponi, M., Vuagniaux, G., Wattenhofer, M., Shibuya, K., Vazquez, M., Dougherty, L., Scamuffa, N., Guida, E., Okui, M., Rossier, C., Hancock, M., Buchet, K., Reymond, A., Hummler, E., Marzella, P. L., Kudoh, J., Shimizu, N., Scott, H. S., Antonarakis, S. E., and Rossier, B. C. (2002) *Hum. Mol. Genet.* **11,** 2829–2836
10. Peters, T. A., Levtchenko, E., Cremers, C. W., Curfs, J. H., and Monnens, L. A. (2006) *Acta Otolaryngol.* **126,** 237–239
11. Bourane, S., Garces, A., Venteo, S., Pattyn, A., Hubert, T., Fichard, A., Puech, S., Boukhaddaoui, H., Baudet, C., Takahashi, S., Valmier, J., and Carroll, P. (2009) *Neuron* **64,** 857–870
12. Ladrech, S., Guitton, M., Saido, T., and Lenoir, M. (2004) *J. Comp. Neurol.*

477, 149–160
13. Ou, H. C., Harding, G. W., and Bohne, B. A. (2000) *Hear Res.* **145,** 123–129
14. Brugeaud, A., Travo, C., Demêmes, D., Lenoir, M., Llorens, J., Puel, J. L., and Chabbert, C. (2007) *J. Neurosci.* **27,** 3503–3511
15. Boadas-Vaello, P., Riera, J., and Llorens, J. (2005) *Toxicol. Sci.* **88,** 456–466
16. Ahmed, Z. M., Li, X. C., Powell, S. D., Riazuddin, S., Young, T. L., Ramzan, K., Ahmad, Z., Luscombe, S., Dhillon, K., MacLaren, L., Ploplis, B., Shotland, L. I., Ives, E., Riazuddin, S., Friedman, T. B., Morell, R. J., and Wilcox, E. R. (2004) *BMC Med. Genet.* **5,** 24
17. Shnerson, A., Lenoir, M., van de Water, T. R., and Pujol, R. (1983) *Brain Res.* **285,** 305–315
18. Aran, J. M., Erre, J. P., Guilhaume, A., and Aurousseau, C. (1982) *Acta Otolaryngol. Suppl.* **390,** 1–30
19. Wang, J., Van De Water, T. R., Bonny, C., de Ribaupierre, F., Puel, J. L., and Zine, A. (2003) *J. Neurosci.* **23,** 8596–8607
20. Kraus, H. J., and Aulbach-Kraus, K. (1981) *Hear. Res.* **4,** 89–102
21. Beraneck, M., McKee, J. L., Aleisa, M., and Cullen, K. E. (2008) *J. Neurophysiol.* **100,** 945–958
22. Géléoc, G. S., and Holt, J. R. (2003) *Nat. Neurosci.* **6,** 1019–1020
23. Lee, Y. J., Park, D., Kim, S. Y., and Park, W. J. (2003) *J. Med. Genet.* **40,** 629–631
24. Gründer, S., Müller, A., and Ruppersberg, J. P. (2001) *Eur. J. Neurosci.* **13,** 641–648
25. Zhong, S. X., and Liu, Z. H. (2004) *Hear. Res.* **193,** 1–8
26. Couloigner, V., Fay, M., Djelidi, S., Farman, N., Escoubet, B., Runembert, I., Sterkers, O., Friedlander, G., and Ferrary, E. (2001) *Am. J. Physiol. Renal Physiol.* **280,** F214–F222
27. Guipponi, M., Tan, J., Cannon, P. Z., Donley, L., Crewther, P., Clarke, M., Wu, Q., Shepherd, R. K., and Scott, H. S. (2007) *Am. J. Pathol.* **171,** 608–616
28. Bugge, T. H., Antalis, T. M., and Wu, Q. (2009) *J. Biol. Chem.* **284,** 23177–23181
29. Altamura, S., D'Alessio, F., Selle, B., and Muckenthaler, M. U. (2010) *Biochem. J.* **431,** 363–371
30. Velasco, G., Cal, S., Quesada, V., Sánchez, L. M., and López-Otín, C. (2002) *J. Biol. Chem.* **277,** 37637–37646
31. Behrens, M., Bufe, B., Schmale, H., and Meyerhof, W. (2004) *Cell Mol. Life Sci.* **61,** 2866–2877
32. Desai, S. S., Zeh, C., and Lysakowski, A. (2005) *J. Neurophysiol.* **93,** 251–266